

Probing extra Yukawa couplings by precision measurements of Higgs properties

Wei-Shu Hou and Mariko Kikuchi

Department of Physics, National Taiwan University, Taipei 10617, Taiwan

(Dated: October 23, 2018)

If one removes any *ad hoc* symmetry assumptions, the general two Higgs doublet model should have additional Yukawa interactions independent from fermion mass generation, in general involving flavor changing neutral Higgs couplings. These extra couplings can affect the discovered Higgs boson h through fermion loop contributions. We calculate the renormalized hZZ coupling at one-loop level and evaluate the dependence on heavy Higgs boson mass and extra Yukawa coupling ρ_{tt} . Precision measurements at future colliders can explore the parameter space, and can give stronger bound on ρ_{tt} than the current bound from flavor experiments. As a side result, we find that if $\rho_{tt} \cos \gamma < 0$, where $\cos \gamma$ is the exotic Higgs component of h , the ρ_{tt} -induced top loop contribution cancels against bosonic loop contributions, and one may have alignment without decoupling, namely $\sin(-\gamma) \simeq 1$, but exotic scalar bosons could have masses at several hundred GeV.

I. INTRODUCTION

The LHC has firmly established the 125 GeV Higgs boson (h), and all data so far are consistent [1, 2] with the predictions of the Standard Model (SM). But, within measurement errors, this certainly does not mean that the Higgs sector must be minimal within SM. There is no theoretical principle that requires the Higgs sector to be composed of only one weak isodoublet, and it may well be extended beyond the minimal.

With the existence of one doublet established, the two Higgs doublet model (2HDM) is one of the simplest and most reasonable extensions of the Higgs sector, and often appears in beyond SM new physics models, such as supersymmetry (SUSY). There are various types of 2HDMs, the most popular are those with a softly broken Z_2 symmetry [3], which forbids flavor changing neutral Higgs (FCNH) couplings. The so-called 2HDM II, where each charge type of quarks receive mass from their own separate Higgs doublet, automatically arises with SUSY. In part because of this, theoretical and phenomenological properties of 2HDMs with Z_2 symmetry have been studied extensively in the literature [4]. However, since the Z_2 symmetry is *ad hoc*, the Yukawa matrices may become too restrictive “artificially”. In the LHC era, the additional Yukawa interactions should not be determined by such *ad hoc* symmetries, but by experiments in a bottom-up approach. After all, so far there is no indication of SUSY at the LHC.

If the Higgs sector is extended to two Higgs doublets, Φ and Φ' , there are in general two Yukawa interaction matrices for each type of fermion charge. As one can always rotate to the basis where only one scalar doublet develops a vacuum expectation value (VEV), the Yukawa matrix for the Higgs field with non-zero VEV gives the mass matrix, hence gets automatically diagonalized, and these masses and Yukawa couplings are now well measured. However, the second Yukawa matrix (ρ_{ij}^f with $f = u, d, e$), i.e. the Yukawa matrix for the scalar field without a VEV, gives rise to additional Yukawa interactions of the exotic scalar doublet, which would naturally contain FCNH couplings. While it was the latter cou-

plings that lead Glashow and Weinberg to impose discrete symmetries [3] to forbid them, it was subsequently pointed out that Nature exhibits a fermion flavor and mass pattern [5, 6] that may not forbid FCNH couplings involving the third generation [7], and 2HDM without Z_2 symmetry was called 2HDM III. We shall just call it the general 2HDM. Some of the most striking signatures of the scenario are $t \rightarrow ch$ [7, 8] or $h \rightarrow \mu\tau$ decays [9].

Most components of the second Yukawa matrices have been strongly constrained by various flavor experiments. However, some components are still allowed to be $\mathcal{O}(1)$. For example, the strongest constraint on $\rho_{tt} \equiv \rho_{33}^u$ is given by $\bar{B}_{d,s}^0 - B_{d,s}^0$ mixing, but $\rho_{tt} \sim 1$ is allowed [10]. In this paper, we do not address FCNH couplings, but would like to suggest indirect detection of the additional Yukawa interactions via precision measurements of Higgs boson h couplings at future colliders. The effect of additional Yukawa interactions such as ρ_{tt} appears as deviations in Higgs boson couplings from SM prediction. Measurement accuracies will be dramatically improved in the future, first at the high luminosity LHC (HL-LHC), and subsequently at the International Linear Collider (ILC). For example, an expected uncertainty (1σ) of the hZZ coupling is $\mathcal{O}(1\%)$ [11, 12] and $\mathcal{O}(0.1\%)$ [11] at the HL-LHC and ILC, respectively. Such precision measurements can probe coupling deviations due to the extra Yukawa interactions.

We calculate the renormalized hZZ coupling at the one-loop level in the on-shell and minimal subtraction scheme. Although the one-loop correction to Higgs boson couplings have been well studied in the 2HDMs with Z_2 symmetry [13–20], such is not the case for the general 2HDM. We evaluate not only fermion loop contributions, but also scalar and vector boson loop contributions. This paper focuses on the top quark loop contributions to the hZZ couplings as a simple first step. We evaluate numerically the dependence of hZZ coupling on the heavy Higgs boson mass and additional Yukawa coupling parameter ρ_{tt} , and elucidate “alignment without decoupling” [23–25] that the general 2HDM could harbor. That is, when the top loop contribution cancels against the bosonic loop contributions, one could have

alignment (h is close to SM Higgs) without pushing the extra Higgs bosons to become superheavy. We illustrate what parameter space in ρ_{tt} the HL-LHC and ILC precision measurements can explore for several heavy Higgs boson masses. We discuss whether the precision measurements can give stronger bound on ρ_{tt} than the current bound from B_d^0 and B_s^0 mixings, and the constraint from future prospects for new scalar boson search at the LHC.

This paper is organized as follows. In Sec. II and III, we briefly review the tree level properties of the 2HDM Higgs potential and the Yukawa interaction, respectively, to fix notation and motivate our study. We present our calculational scheme in Sec. IV for one-loop corrections to the Higgs boson couplings in the general 2HDM. In Sec. V, we numerically study the deviation in hZZ coupling as a function of ρ_{tt} and extra scalar boson masses, as well as dependence on Higgs mixing, and then compare with future precision measurement sensitivities. Conclusion is given in Sec. VI, while various formulae are collected in an Appendix.

II. HIGGS POTENTIAL

The Higgs potential of the general two Higgs doublet model (2HDM) is given by

$$\begin{aligned}
V = & \mu_{11}^2 |\Phi|^2 + \mu_{22}^2 |\Phi'|^2 - (\mu_{12}^2 \Phi^\dagger \Phi' + h.c.) \\
& + \frac{\eta_1}{2} |\Phi|^4 + \frac{\eta_2}{2} |\Phi'|^4 + \eta_3 |\Phi|^2 |\Phi'|^2 + \eta_4 (\Phi^\dagger \Phi') (\Phi'^\dagger \Phi) \\
& + \left\{ \frac{\eta_5}{2} (\Phi^\dagger \Phi')^2 + (\eta_6 |\Phi|^2 + \eta_7 |\Phi'|^2) (\Phi^\dagger \Phi') + h.c. \right\},
\end{aligned} \tag{1}$$

where μ_{12}^2 , η_5 , η_6 and η_7 can be complex, while the latter two are absent from 2HDM with Z_2 symmetries. The two doublet fields can be parameterized as

$$\begin{aligned}
\Phi &= \begin{pmatrix} G^+ \\ \frac{1}{\sqrt{2}}(\phi_1 + v + iG^0) \end{pmatrix}, \\
\Phi' &= \begin{pmatrix} H^+ \\ \frac{1}{\sqrt{2}}(\phi_2 + iA) \end{pmatrix}.
\end{aligned} \tag{2}$$

where, without loss of generality [26, 27], Φ is taken as the one with non-zero vacuum expectation value (VEV), while Φ' has no VEV.

After imposing the minimization conditions, μ_{11}^2 and μ_{12}^2 are expressed in terms of other parameters as

$$\mu_{11}^2 = -\frac{\eta_1}{2} v^2, \quad \mu_{12}^2 = \frac{\eta_6}{2} v^2, \tag{3}$$

and the mass terms of the Higgs potential become

$$\begin{aligned}
V_{\text{mass}} = & (\phi_1, \phi_2) M_{\text{even}}^2 \begin{pmatrix} \phi_1 \\ \phi_2 \end{pmatrix} + (G^0, A) M_{\text{odd}}^2 \begin{pmatrix} G^0 \\ A \end{pmatrix} \\
& + (G^-, H^-) M_{\pm}^2 \begin{pmatrix} G^+ \\ H^+ \end{pmatrix},
\end{aligned} \tag{4}$$

where the CP-odd M_{odd}^2 and the charged M_{\pm}^2 matrices are diagonal, with nonzero eigenvalues given by

$$m_A^2 = \mu_{22}^2 + \frac{v^2}{2} (\eta_3 + \eta_4 - \eta_5), \tag{5}$$

$$m_{H^\pm}^2 = \mu_{22}^2 + \frac{\eta_3}{2} v^2. \tag{6}$$

For the CP-even M_{even}^2 matrix, one has

$$M_{\text{even}}^2 = \begin{pmatrix} \eta_1 v^2 & \eta_6 v^2 \\ \eta_6 v^2 & \mu_{22}^2 + \frac{v^2}{2} (\eta_3 + \eta_4 + \eta_5) \end{pmatrix}, \tag{7}$$

which is diagonalized by the rotation matrix R with mixing angle γ ,

$$\begin{aligned}
R^T(\gamma) M_{\text{even}}^2 R(\gamma) &= \begin{pmatrix} m_H^2 & 0 \\ 0 & m_h^2 \end{pmatrix}, \\
R(\gamma) &= \begin{pmatrix} \cos \gamma & -\sin \gamma \\ \sin \gamma & \cos \gamma \end{pmatrix},
\end{aligned} \tag{8}$$

where we keep the convention of 2HDM II, and H , h are CP-even mass eigenstates. The mixing angle γ is expressed by

$$\begin{aligned}
& \sin 2\gamma \\
&= \frac{2\eta_6 v^2}{\sqrt{[v^2(2\eta_1 - \eta_3 - \eta_4 - \eta_5)/2 - \mu_{22}^2]^2 + 4(\eta_6 v^2)^2}}.
\end{aligned} \tag{9}$$

The isospin states ϕ_1 and ϕ_2 are related to the mass eigenstates H and h by

$$\begin{pmatrix} \phi_1 \\ \phi_2 \end{pmatrix} = R(\gamma) \begin{pmatrix} H \\ h \end{pmatrix}, \tag{10}$$

where h is the 125 GeV boson, and $\sin \gamma \rightarrow -1$ corresponds to the SM, or alignment limit. For the decoupling limit in which the extra Higgs bosons are much heavier than the electroweak scale, i.e. $\varepsilon \equiv v^2/m_{H,A,H^\pm}^2 \ll 1$, the mixing angle γ can be approximated by

$$\cos \gamma \simeq F_{\text{Sign}} \varepsilon + \mathcal{O}(\varepsilon^2), \quad (\text{decoupling}) \tag{11}$$

where F_{Sign} is the sign of $\sin \gamma$.

In summary, some parameters in the Higgs potential of Eq. (1) are rewritten with physical parameters as

$$\eta_1 = \frac{1}{v^2} (m_H^2 c_\gamma^2 + m_h^2 s_\gamma^2), \tag{12}$$

$$\eta_3 = -\frac{2}{v^2} (\mu_{22}^2 - m_{H^\pm}^2), \tag{13}$$

$$\begin{aligned}
\eta_4 = \frac{1}{2v^2} (2m_A^2 - 4m_{H^\pm}^2 + m_h^2 + m_H^2 \\
+ (m_h^2 - m_H^2) c_{2\gamma}),
\end{aligned} \tag{14}$$

$$\eta_5 = \frac{1}{2v^2} (-2m_A^2 + m_h^2 + m_H^2 + (m_h^2 - m_H^2) c_{2\gamma}), \tag{15}$$

$$\eta_6 = \frac{s_\gamma c_\gamma}{v^2} (-m_h^2 + m_H^2), \tag{16}$$

where $s_\gamma = \sin \gamma$ (and likewise for $c_\gamma, c_{2\gamma}$), and

$$\mu_{11}^2 = -\frac{1}{2}(m_h^2 s_\gamma^2 + m_H^2 c_\gamma^2), \quad (17)$$

$$\mu_{12}^2 = -\frac{s_{2\gamma}}{4}(m_h^2 - m_H^2). \quad (18)$$

Note that η_2, η_7 and μ_{22}^2 remain as free parameters, as they cannot be expressed in terms of mass and mixing parameters as above. Altogether, there are 9 independent parameters in the potential.

Dimensionless parameters of the Higgs potential are restricted by theoretical constraints. In this paper, we take into account the following constraints:

- **Perturbativity**

The perturbative bound requires that all dimensionless parameters be smaller than some criterion constants, i.e. $\eta_i \leq \xi_i$, $i = 1 - 7$. In all analyses in this paper, we take $\xi_i = 2$. While somewhat arbitrary, the point is to keep Higgs parameters in perturbative realm.

- **Vacuum stability**

The vacuum stability bound means the potential should be bounded from below in all field directions. This requires the value of the potential to be positive at large $|\Phi|$ and $|\Phi'|$. In the analyses of this paper, we use the vacuum stability condition given in Ref. [28].

III. YUKAWA INTERACTIONS

In this section, we discuss the Yukawa interaction.

A. Exotic Yukawas and the alignment limit

The general Yukawa Lagrangian for 2HDM is

$$\begin{aligned} -\mathcal{L}_{\text{Yukawa}} = & \bar{Q}_{L,i}(V_{\text{CKM}}^\dagger)_{il} \left(\kappa_{u_l u_j} \tilde{\Phi} + \rho_{u_l u_j} \tilde{\Phi}' \right) u_{R,j} \\ & + \bar{Q}_{L,i} \left(\kappa_{d_i d_j} \Phi + \rho_{d_i d_j} \Phi' \right) d_{R,j} \\ & + \bar{L}_{L,i} \left(\kappa_{e_i e_j} \Phi + \rho_{e_i e_j} \Phi' \right) e_{R,j} + h.c., \quad (19) \end{aligned}$$

with

$$Q_{L,i} = \begin{pmatrix} (V_{\text{CKM}}^\dagger)_{ij} u_{L,j} \\ d_{L,i} \end{pmatrix}, \quad L_{L,i} = \begin{pmatrix} (V_{\text{MNS}}^\dagger)_{ij} \nu_{L,j} \\ e_{L,i} \end{pmatrix}, \quad (20)$$

where V_{CKM} and V_{MNS} are the Kobayashi-Maskawa and Maki-Nakagawa-Sakata matrices, respectively. In Eq. (19), $\kappa_{f_i f_j}$ multiplied by v corresponds to the mass matrix as $m_{ij} = \delta_{ij} \kappa_{f_i f_i} v / \sqrt{2}$, because only Φ gives VEV. On the other hand, $\rho_{f_i f_j}$ are the additional Yukawa interactions of the exotic doublet Φ' , which are in general

not diagonal. Rather than imposing a Z_2 symmetry [3] to eliminate off-diagonal FCNH couplings, the viewpoint promoted here is that they should be as constrained by data, which is why we call this the general 2HDM.

If $\rho_{f_i f_j}$ are Hermitian matrices, the interaction terms in the mass basis are

$$\begin{aligned} \mathcal{L}_{\text{Yukawa}} = & \bar{f}_i \lambda_{h f_i f_j} h f_j + \bar{f}_i \lambda_{H f_i f_j} H f_j + i \bar{f}_i \lambda_{A f_i f_j} A \gamma_5 f_j \\ & - [\bar{u}_i (V_{\text{CKM}} \rho^d P_R - \rho^{u\dagger} V_{\text{CKM}} P_L)_{ij} H^+ d_j \\ & + \bar{\nu}_{L,i} (V_{\text{MNS}} \rho^e)_{ij} H^+ e_{R,j} + h.c.], \quad (21) \end{aligned}$$

where

$$\lambda_{h f_i f_j} = -\frac{m_{f_i}}{v} \sin(-\gamma) \delta_{ij} - \frac{\rho_{f_i f_j}}{\sqrt{2}} \cos \gamma, \quad (22)$$

$$\lambda_{H f_i f_j} = -\frac{m_{f_i}}{v} \cos \gamma \delta_{ij} + \frac{\rho_{f_i f_j}}{\sqrt{2}} \sin(-\gamma), \quad (23)$$

$$\lambda_{A f f} = \frac{\rho_{f_i f_j}}{\sqrt{2}}. \quad (24)$$

As all evidence support h to be consistent with the Higgs boson of the SM, we consider Yukawa coupling constants close to the alignment limit. That is, we introduce a parameter x defined as

$$\gamma = -\frac{\pi}{2} + x, \quad (25)$$

where $x \rightarrow 0$ corresponds to the alignment limit. In this limit, the coefficients $\lambda_{\phi f_i f_j}$ of the Yukawa interaction vertex $\phi \bar{f}_i f_j$ can be approximated by

$$\lambda_{h f_i f_j} = -\frac{m_{f_i}}{v} \delta_{ij} - \frac{x}{\sqrt{2}} \rho_{f_i f_j} + \mathcal{O}(x^2), \quad (26)$$

$$\lambda_{H f_i f_j} = \frac{1}{\sqrt{2}} \rho_{f_i f_j} - \frac{m_{f_i}}{v} \delta_{ij} x + \mathcal{O}(x^2), \quad (27)$$

$$\lambda_{A f_i f_j} = \frac{1}{\sqrt{2}} \rho_{f_i f_j} \gamma_5 + \mathcal{O}(x^2). \quad (28)$$

While h does pick up a small component of exotic couplings (including FCNH), in this paper, we shall mostly be interested in the extra ρ_{tt} coupling of exotic Higgs bosons, where we have dropped the u quark superscript.

We would like to mention the difference between x and ε , which is introduced in the previous section. While $x \rightarrow 0$ is the alignment limit, the limit $\varepsilon \rightarrow 0$ means the decoupling of the heavy exotic bosons. As can be seen from Eq. (11), decoupling is a special case of alignment.

B. Experimental constraints on ρ_{tt}

Elements of ρ_{ij}^f for down type quarks and charged leptons are constrained rather strongly by various B meson decay and lepton flavor violation processes [29]. One should, however, keep an eye on $\rho_{23}^e \equiv \rho_{\mu\tau}$, which can generate $h \rightarrow \mu\tau$ [9] with Yukawa coupling strength $\rho_{\mu\tau} x$ via Eq. (26). A hint from 8 TeV data by CMS [30] might

reappear in the 2016 data set at 13 TeV that is much larger than obtained in 2015. Similarly, $\rho_{23}^u \equiv \rho_{ct}$ may generate $t \rightarrow ch$ decay [7, 8], which is being pursued at the LHC [31, 32]. We note that if these decays are absent, it does not necessarily imply small $\rho_{\mu\tau}$ and ρ_{ct} , but may reflect the alignment limit of $x \sim 0$.

We are mainly interested in the extra diagonal coupling ρ_{tt} of the exotic Higgs H , as the SM Yukawa coupling $\lambda_t \equiv \kappa_{tt} \simeq 1$ for h is the largest known coupling. The current bound on ρ_{tt} comes mainly from $B_{d,s}$ mixing and $B \rightarrow X_s \gamma$. It is found [10] that the latest B_s mixing data gives the 95% C.L. bound $|\rho_{tt}| < 1$ ($-0.35 < \rho_{tt} < 0.2$) for $\rho_{ct} = 0$ ($\rho_{ct} = 0.1$), for charged Higgs boson mass $m_{H^+} = 500$ GeV. For $m_{H^+} = 500$ GeV and $\rho_{ct} = 0$, the region with $\rho_{tt} < -1$ and $0.6 < \rho_{tt}$ for $\rho_{bb} = \kappa_{bb}$ has been excluded by data on the $B \rightarrow X_s \gamma$ process. However, if $|\rho_{bb}|$ is less than about 0.005, ρ_{tt} is practically not constrained. In any case and for our purpose, if we consider the situation where all components of ρ_{ij}^f matrices are zero except for ρ_{tt} , the strongest bound is $|\rho_{tt}| < 1$ [10] (for $m_{H^+} = 500$ GeV), which comes from B_s mixing. It is intriguing that the second top Yukawa coupling could be as strong as the SM Higgs boson.

Collider experiments can in principle provide constraints on ρ_{tt} by direct search of the heavy scalar bosons. Unfortunately, while mass bounds on exotic vector bosons have been pursued in $t\bar{t}$ resonance searches [33, 34], the situation is unclear when it comes to heavy scalars. This is due to interference with the production of such a boson, which involves the top quark in the triangle loop as a consequence of $\rho_{tt} \neq 0$.

The situation for heavy Higgs boson search through $gg \rightarrow S \rightarrow t\bar{t}$ process at the LHC has been assessed recently in Ref. [35], where the expected 95% C.L. exclusion limits on the top quark Yukawa coupling of additional CP-even and CP-odd scalar bosons are evaluated assuming several LHC scenarios. Although the simplified model in Ref. [35] is not the same as the general 2HDM, for $\cos \gamma \simeq 0$, i.e. $x \simeq 0$, the results can be applied to the general 2HDM. For LHC at 13 TeV collision energy and integrated luminosity of 30 fb^{-1} (i.e. 2016 data), one could survey the region of $\rho_{tt} > 2.4$ by using the $A \rightarrow t\bar{t}$ process for $m_A = 500$ GeV. For 300 fb^{-1} , the expected bound is improved to $\rho_{tt} > 1.4$ ($\rho_{tt} > 2.6$) for $m_A = 500$ GeV (1 TeV) using conservative assumptions for efficiency and systematic uncertainty, and $\rho_{tt} > 0.5$ ($\rho_{tt} > 0.9$) for $m_A = 500$ GeV (1 TeV) using more aggressive assumptions. In the case where A is heavier, the exclusion limit on ρ_{tt} becomes further relaxed.

It is in part this difficulty of probing ρ_{tt} directly at LHC via $t\bar{t}$ scalar resonances that motivates our indirect, precision measurement approach.

IV. RENORMALIZATION

We now discuss renormalization of the scalar sector, towards the indirect, precision measurement approach.

A. Parameter shift

As mentioned in Sec. II, there are 9 independent parameters,

$$m_h^2, m_H^2, m_A^2, m_{H^\pm}^2, \gamma, v, \mu_{22}^2, \eta_2, \eta_7, \quad (29)$$

which get shifted by

$$m_\phi^2 \rightarrow m_\phi^2 + \delta m_\phi^2, \quad (\phi = h, H, A, \text{ and } H^\pm), \quad (30)$$

$$\gamma \rightarrow \gamma + \delta\gamma, \quad v \rightarrow v + \delta v, \quad \mu_{22}^2 \rightarrow \mu_{22}^2 + \delta\mu_{22}^2, \quad (31)$$

$$\eta_2 \rightarrow \eta_2 + \delta\eta_2, \quad \eta_7 \rightarrow \eta_7 + \delta\eta_7. \quad (32)$$

The CP-even, CP-odd and charged components of the doublet fields are corrected by

$$\begin{aligned} \begin{pmatrix} \phi_1 \\ \phi_2 \end{pmatrix} &\rightarrow \tilde{Z}_{\text{even}} \begin{pmatrix} \phi_1 \\ \phi_2 \end{pmatrix}, \quad \begin{pmatrix} G^0 \\ A \end{pmatrix} \rightarrow \tilde{Z}_{\text{odd}} \begin{pmatrix} G^0 \\ A \end{pmatrix}, \\ \begin{pmatrix} G^\pm \\ H^\pm \end{pmatrix} &\rightarrow \tilde{Z}_\pm \begin{pmatrix} G^\pm \\ H^\pm \end{pmatrix}, \end{aligned} \quad (33)$$

where \tilde{Z}_{even} , \tilde{Z}_{odd} and \tilde{Z}_\pm are real 2×2 matrices. We here define \tilde{Z}_{odd} and \tilde{Z}_\pm as follows,

$$\tilde{Z}_{\text{odd}} = \begin{pmatrix} 1 + \frac{1}{2}\delta Z_{G^0} & \delta C_{GA} \\ \delta C_{AG} & 1 + \frac{1}{2}\delta Z_A \end{pmatrix}, \quad (34)$$

$$\tilde{Z}_\pm = \begin{pmatrix} 1 + \frac{1}{2}\delta Z_{G^\pm} & \delta C_{GH} \\ \delta C_{HG} & 1 + \frac{1}{2}\delta Z_{H^\pm} \end{pmatrix}. \quad (35)$$

For CP-even states, from Eqs. (10) and (33), the relation between bare mass eigenstates and renormalized mass eigenstates can be derived as

$$\begin{aligned} \begin{pmatrix} H \\ h \end{pmatrix}_B &= R(-\gamma)_B \tilde{Z}_{\text{even}} \begin{pmatrix} \phi_1 \\ \phi_2 \end{pmatrix} \\ &= R(-\delta\gamma)R(-\gamma) \tilde{Z}_{\text{even}} R(\gamma) \begin{pmatrix} H \\ h \end{pmatrix} \\ &= R(-\delta\gamma) Z_{\text{even}} \begin{pmatrix} H \\ h \end{pmatrix}. \end{aligned} \quad (36)$$

where Z_{even} is defined as,

$$Z_{\text{even}} = \begin{pmatrix} 1 + \frac{1}{2}\delta Z_H & \delta C_{Hh} \\ \delta C_{hH} & 1 + \frac{1}{2}\delta Z_h \end{pmatrix}. \quad (37)$$

Therefore, CP-even mass eigenstates are shifted as

$$\begin{pmatrix} H \\ h \end{pmatrix} \rightarrow \begin{pmatrix} 1 + \frac{1}{2}\delta Z_H & \delta C_{Hh} + \delta\gamma \\ \delta C_{hH} - \delta\gamma & 1 + \frac{1}{2}\delta Z_h \end{pmatrix} \begin{pmatrix} H \\ h \end{pmatrix}. \quad (38)$$

We emphasize that mixing counterterms δC_{XY} are not symmetric, i.e. $\delta C_{Hh} \neq \delta C_{hH}$.

In addition to the above parameters, counterterms of two tadpoles for ϕ_1 and ϕ_2 should be introduced at higher order,

$$T_1 \rightarrow T_1 + \delta T_1, \quad T_2 \rightarrow T_2 + \delta T_2, \quad (39)$$

where T_1 and T_2 on the right-hand sides have to become zero by minimization conditions of the Higgs potential. Therefore, the renormalized tadpoles are

$$\hat{T}_1 = \delta T_1 + T_1^{1\text{PI}}, \quad (40)$$

$$\hat{T}_2 = \delta T_2 + T_2^{1\text{PI}}, \quad (41)$$

where $T_i^{1\text{PI}}$ are the one particle irreducible (1PI) diagram contributions to the tadpole of ϕ_i . Explicit forms of their fermion loop contributions are given in the Appendix.

B. Renormalized two-point functions

The renormalized two point functions $\hat{\Pi}_{XY}$ are expressed as

$$\begin{aligned} \hat{\Pi}_{hh}[p^2] &= (p^2 - m_h^2)\delta Z_h - \delta m_h^2 + \frac{s_\gamma^2}{v}\delta T_1 \\ &\quad - \frac{2s_\gamma c_\gamma}{v}\delta T_2 + \Pi_{hh}^{1\text{PI}}[p^2], \end{aligned} \quad (42)$$

$$\begin{aligned} \hat{\Pi}_{HH}[p^2] &= (p^2 - m_H^2)\delta Z_H - \delta m_H^2 + \frac{c_\gamma^2}{v}\delta T_1 \\ &\quad + \frac{2s_\gamma c_\gamma}{v}\delta T_2 + \Pi_{HH}^{1\text{PI}}[p^2], \end{aligned} \quad (43)$$

$$\hat{\Pi}_{AA}[p^2] = (p^2 - m_A^2)\delta m_A^2 - \delta m_A^2 + \Pi_{AA}^{1\text{PI}}[p^2], \quad (44)$$

$$\hat{\Pi}_{H^+H^-}[p^2] = (p^2 - m_{H^\pm}^2)\delta Z_{H^\pm} - \delta m_{H^\pm}^2 + \Pi_{H^+H^-}^{1\text{PI}}[p^2]. \quad (45)$$

Renormalized scalar mixing effects are given by

$$\begin{aligned} \hat{\Pi}_{hH}[p^2] &= p^2(\delta C_{hH} + \delta C_{Hh}) + m_h^2(\delta\gamma - \delta C_{hH}) \\ &\quad - m_H^2(\delta\gamma + \delta C_{Hh}) \\ &\quad - \frac{s_\gamma c_\gamma}{v}\delta T_1 + \frac{c_{2\gamma}}{v}\delta T_2 + \Pi_{hH}^{1\text{PI}}[p^2], \end{aligned} \quad (46)$$

$$\begin{aligned} \hat{\Pi}_{AG}[p^2] &= p^2(\delta C_{AG} + \delta C_{GA}) - m_A^2\delta C_{AG} + \frac{1}{v}\delta T_2 \\ &\quad + \Pi_{AG}^{1\text{PI}}[p^2], \end{aligned} \quad (47)$$

$$\begin{aligned} \hat{\Pi}_{HG}[p^2] &= p^2(\delta C_{HG} + \delta C_{GH}) - m_{H^\pm}^2\delta C_{HG} + \frac{1}{v}\delta T_2 \\ &\quad + \Pi_{HG}^{1\text{PI}}[p^2]. \end{aligned} \quad (48)$$

C. Renormalization conditions

In this subsection, we discuss how the counterterms can be determined by the renormalization conditions.

We determine the counterterms of tadpoles by the following conditions,

$$\hat{T}_h = 0, \quad \hat{T}_H = 0, \quad (49)$$

hence

$$\delta T_h = -T_h^{1\text{PI}}, \quad \delta T_H = -T_H^{1\text{PI}}, \quad (50)$$

where $\delta T_{h,H}$ are related to $\delta T_{1,2}$ as,

$$\begin{pmatrix} \delta T_1 \\ \delta T_2 \end{pmatrix} = R(\gamma) \begin{pmatrix} \delta T_h \\ \delta T_H \end{pmatrix}. \quad (51)$$

Mass counterterms are determined by imposing on-shell conditions to renormalized two-point functions, Eqs. (42)-(45), as follows

$$\hat{\Pi}_{\phi\phi}[m_\phi^2] = 0. \quad (52)$$

The counterterms are then given by

$$\delta m_h^2 = \frac{s_\gamma^2}{v}\delta T_1 - \frac{2s_\gamma c_\gamma}{v}\delta T_2 + \Pi_{hh}^{1\text{PI}}[m_h^2], \quad (53)$$

$$\delta m_H^2 = \frac{c_\gamma^2}{v}\delta T_1 + \frac{2s_\gamma c_\gamma}{v}\delta T_2 + \Pi_{HH}^{1\text{PI}}[m_H^2], \quad (54)$$

$$\delta m_A^2 = \Pi_{AA}^{1\text{PI}}[m_A^2], \quad (55)$$

$$\delta m_{H^\pm}^2 = \Pi_{H^+H^-}^{1\text{PI}}[m_{H^\pm}^2]. \quad (56)$$

By imposing the following conditions;

$$\begin{aligned} \left. \frac{d}{dp^2} \hat{\Pi}_{\phi\phi}[p^2] \right|_{p^2=m_\phi^2} &= 0, \quad \left. \frac{d}{dp^2} \hat{\Pi}_{G^0G^0}[p^2] \right|_{p^2=m_{G^0}^2} = 0, \\ \left. \frac{d}{dp^2} \hat{\Pi}_{G^+G^-}[p^2] \right|_{p^2=m_{G^\pm}^2} &= 0, \end{aligned} \quad (57)$$

wave function renormalization is fixed as

$$\delta Z_\phi = - \left. \frac{d}{dp^2} \Pi_{\phi\phi}^{1\text{PI}}[p^2] \right|_{p^2=m_\phi^2}, \quad (58)$$

$$\delta Z_{G^0} = - \left. \frac{d}{dp^2} \Pi_{G^0G^0}^{1\text{PI}}[p^2] \right|_{p^2=m_{G^0}^2}, \quad (59)$$

$$\delta Z_{G^\pm} = - \left. \frac{d}{dp^2} \Pi_{G^\pm G^\pm}^{1\text{PI}}[p^2] \right|_{p^2=m_{G^\pm}^2}. \quad (60)$$

We impose the following conditions to mixing two-point functions of renormalized fields,

$$\hat{\Pi}_{AG}[m_A^2] = \hat{\Pi}_{AG}[0] = 0, \quad \hat{\Pi}_{HG}[m_{H^\pm}^2] = \hat{\Pi}_{HG}[0] = 0, \quad (61)$$

such that mass eigenstates are diagonalized on mass shell. This determines the renormalization conditions for δC_{AG} , δC_{GA} , δC_{HG} and δC_{GH} ,

$$\delta C_{AG} = \frac{1}{m_A^2} \left(\frac{\delta T_2}{v} + \Pi_{AG}^{1\text{PI}}[0] \right), \quad (62)$$

$$\delta C_{GA} = \frac{1}{m_A^2} \left(-\frac{\delta T_2}{v} - \Pi_{AG}^{1\text{PI}}[m_A^2] \right), \quad (63)$$

$$\delta C_{HG} = \frac{1}{m_{H^\pm}^2} \left(\frac{\delta T_2}{v} + \Pi_{HG}^{1\text{PI}}[0] \right), \quad (64)$$

$$\delta C_{GH} = \frac{1}{m_{H^\pm}^2} \left(-\frac{\delta T_2}{v} - \Pi_{HG}^{1\text{PI}}[m_{H^\pm}^2] \right). \quad (65)$$

For the CP-even states, as in the case of the CP-odd states, we should impose on-shell condition on the two-point function,

$$\hat{\Pi}_{hH}[m_h^2] = \hat{\Pi}_{hH}[m_H^2] = 0, \quad (66)$$

which leads to the relations between $\delta\gamma$, δC_{hH} and δC_{Hh} :

$$\delta A = \frac{1}{m_H^2 - m_h^2} \left(-\frac{2s_\gamma c_\gamma}{v} \delta T_1 + \frac{2c_{2\gamma}}{v} \delta T_2 + \Pi_{hH}^{1\text{PI}}[m_h^2] + \Pi_{hH}^{1\text{PI}}[m_H^2] \right), \quad (67)$$

$$\delta B = \frac{1}{m_H^2 - m_h^2} (\Pi_{hH}^{1\text{PI}}[m_h^2] - \Pi_{hH}^{1\text{PI}}[m_H^2]), \quad (68)$$

where

$$\delta A \equiv 2\delta\gamma - \delta C_{hH} + \delta C_{Hh}, \quad \delta B \equiv \delta C_{hH} + \delta C_{Hh}. \quad (69)$$

In order to fix the three counterterms $\delta\gamma$, δC_{hH} and δC_{Hh} , an additional condition is required. We employ a minimal subtraction renormalization condition to the three point functions, which requires δC_{hH} to absorb only the divergent part of the HZZ vertex at one-loop level for $p_1^2 = m_Z^2, p_2^2 = m_Z^2, q^2 = m_H^2$,

$$\hat{\Gamma}_{HZZ}^1[m_Z^2, m_Z^2, m_H^2] \Big|_{\text{div. part}} = 0, \quad (70)$$

where $\hat{\Gamma}_{HZZ}^1$ is the scalar part of the HZZ vertex function, as defined through

$$\Gamma_{\varphi ZZ}^{\mu\nu} = \Gamma_{\varphi ZZ}^1 g^{\mu\nu} + \Gamma_{\varphi ZZ}^2 \frac{p_1^\mu p_2^\nu}{m_Z^2} + i\Gamma_{\varphi ZZ}^3 \epsilon^{\mu\nu\rho\sigma} \frac{p_{1,\rho} p_{2,\sigma}}{m_Z^2}. \quad (71)$$

By using Eqs. (67), (68) and the minimal subtraction condition given in Eq. (70), we obtain explicit formulae for $\delta\gamma$, δC_{hH} and δC_{Hh} ,

$$\delta\gamma = \frac{1}{2}(\delta A - \delta B + 2\delta C_{hH}), \quad (72)$$

$$\delta C_{hH} = -\frac{N_f^C s_\gamma}{32\pi^2 v^2} \left\{ c_\gamma (-2m_f^2 + \rho_{ff}^2 v^2 + 2v^2 \rho_{ij} \rho_{ji}) - 2\sqrt{2} v s_\gamma m_f \rho_{ff} \right\} \Delta, \quad (73)$$

$$\delta C_{Hh} = \frac{1}{m_H^2 - m_h^2} (\Pi_{hH}^{1\text{PI}}[m_h^2] - \Pi_{hH}^{1\text{PI}}[m_H^2]) - \delta C_{hH}, \quad (74)$$

where $\Delta \equiv 1/\epsilon - \gamma_E + \ln 4\pi + \ln \mu^2$.

D. Renormalized vertices

The renormalized scalar form factor of the ϕZZ vertex ($\phi = h, H$) is composed of the tree level contribution, the counterterms, and 1PI diagram contributions,

$$\hat{\Gamma}_{\phi ZZ}^1[p_1^2, p_2^2, q^2] = \Gamma_{\phi ZZ}^{\text{tree}} + \delta\Gamma_{\phi ZZ} + \Gamma_{\phi ZZ}^{1,1\text{PI}}[p_1^2, p_2^2, q^2]. \quad (75)$$

The counterterms are given by

$$\delta\Gamma_{hZZ}^1 = \frac{2m_Z^2}{v^2} \sin(-\gamma) \left(\frac{\delta m_Z^2}{m_Z^2} - \frac{\delta v}{v} + \frac{1}{2} \delta Z_h + \delta Z_Z \right) + \frac{2m_Z^2}{v} \cos \gamma \delta C_{Hh}, \quad (76)$$

$$\delta\Gamma_{HZZ}^1 = \frac{2m_Z^2}{v} \cos \gamma \left(\frac{\delta m_Z^2}{m_Z^2} - \frac{\delta v}{v} + \frac{1}{2} \delta Z_H + \delta Z_Z \right) + \frac{2m_Z^2}{v} \sin(-\gamma) \delta C_{hH}, \quad (77)$$

where δm_Z^2 , δZ_Z are the mass counterterm and wave function renormalization of the Z boson, respectively, and their explicit formulae are given in Ref. [15]. We note that Eqs. (76) and (77) have no $\delta\gamma$ dependence, the reason of which can be traced to Eq. (38).

We here define the renormalized scaling factor of the hZZ couplings in the following way;

$$\kappa_Z = \frac{\Gamma_{hZZ}^1[(m_h + m_Z)^2, m_Z^2, m_h^2]}{\Gamma_{hZZ, \text{SM}}^1[(m_h + m_Z)^2, m_Z^2, m_h^2]}, \quad (78)$$

where $\Gamma_{hZZ, \text{SM}}^1$ is the renormalized hZZ coupling function in the SM. We will numerically evaluate the deviation of κ_Z from 1 defined as $\Delta\kappa_Z \equiv \kappa_Z - 1$.

Before we enter numerical calculations, in order to understand parameter dependence of $\Delta\kappa_Z$, we give an approximate formula for the one-loop corrected hZZ coupling that is effective in the decoupling limit, i.e. the limit of $\epsilon \ll 1$. We further expand $\Delta\kappa_Z$ in ϵ :

$$\begin{aligned} \Delta\kappa_Z &\simeq (\sin(-\gamma) - 1) \\ &- \frac{1}{6} \frac{1}{16\pi^2} \sum_{\varphi=H,A,H^\pm} c_\varphi \frac{m_\varphi^2}{v^2} \left(1 - \frac{\mu_{22}^2}{m_\varphi^2} \right)^2 \\ &+ \frac{\sqrt{2} N_t^C}{16\pi^2} \frac{m_t}{v} \rho_{tt} \cos \gamma \sin^2 \gamma \left\{ (2 - \ln[m_H^2]) \right. \\ &- 2 \left[B_0[m_h^2; m_t, m_t] - 4m_t^2 \frac{d}{dp^2} B_0[p^2; m_t, m_t] \Big|_{p^2=m_h^2} \right] \\ &\left. + 2[(v_f^2 + a_f^2)P_1 - (v_f^2 - a_f^2)P_2] \right\} \\ &\simeq -\frac{\eta_6^2}{2} \epsilon^2 - \frac{1}{6} \frac{1}{16\pi^2} \sum_{\varphi=H,A,H^\pm} c_\varphi \frac{m_\varphi^2}{v^2} \left(1 - \frac{\mu_{22}^2}{m_\varphi^2} \right)^2 \\ &- \frac{\sqrt{2} N_t^C}{16\pi^2} \frac{m_t}{v} \rho_{tt} \eta_6 \epsilon \left\{ (2 - \ln[m_H^2]) \right. \\ &- 2 \left[B_0[m_h^2; m_t, m_t] - 4m_t^2 \frac{d}{dp^2} B_0[p^2; m_t, m_t] \Big|_{p^2=m_h^2} \right] \\ &\left. + 2[(v_f^2 + a_f^2)P_1 - (v_f^2 - a_f^2)P_2] \right\} + \frac{1}{16\pi^2} \mathcal{O}(\epsilon^2), \end{aligned} \quad (79)$$

where $c_\varphi = 2$ (1) for $\varphi = H^\pm$ (H, A), $N_t^C (= 3)$ is the color factor of t , B_0 is a Passarino-Veltman loop func-

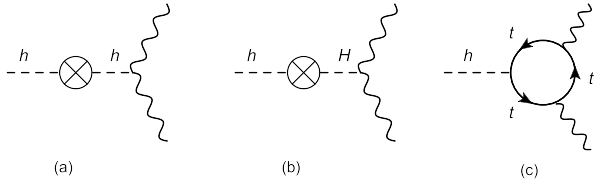


FIG. 1. One loop diagrams contributing to the renormalized hZZ vertex.

tion [31], and $P_{1,2}$ are combinations of various Passarino-Veltman loop functions, defined as,

$$\begin{aligned}
P_1 &\equiv B_0[(m_h + m_Z)^2; m_t, m_t] + B_0[m_Z^2; m_t, m_t] \\
&\quad + 2B_0[m_h^2; m_t, m_t] + (4m_t^2 - m_h^2 - 2m_h m_Z) \\
&\quad \times C_0[(m_h + m_Z)^2, m_Z^2, m_h^2; m_t, m_t, m_t] \\
&\quad - 8C_{24}[(m_h + m_Z)^2, m_Z^2, m_h^2; m_t, m_t, m_t] \\
&\quad \simeq -22.4, \\
P_2 &\equiv B_0[(m_h + m_Z)^2; m_t, m_t] + B_0[m_Z^2; m_t, m_t] \\
&\quad + (4m_t^2 - m_h^2)C_0[(m_h + m_Z)^2, m_Z^2, m_h^2; m_t, m_t, m_t] \\
&\quad \simeq -22.6.
\end{aligned}$$

The first, second and third terms in Eq. (79) correspond to the tree level, extra scalar boson loop and fermion loop contributions, respectively. Small ε is the decoupling limit, which is a special case of alignment.

For the top quark loop contributions enclosed by $\{ \}$ in Eq. (79), the first, second and third terms come from diagrams (a), (b) and (c) in Fig. 1, respectively. Besides ρ_{tt} dependence, these dominant fermion loop contributions have the mixing suppression factor $\cos\gamma$ (or ε). Other contributions coming from fermion loops, such as ρ_{ij}^f ($i \neq j$) contributions, have square or higher power of $\cos\gamma$ (ε) suppression. Thus, contributions from off-diagonal elements of the ρ matrices are subdominant in the alignment limit. In addition, the contributions from all kinds of fermion (f') loops except the top quark are suppressed by $m_{f'}/v$, so that they are also subdominant.

To facilitate our numerical study, let us utilize Eq. (79) to discuss the radiative corrections to κ_Z and $\sin(-\gamma)$. The tree level contribution to the scaling factor κ_Z is

$$\kappa_Z^{\text{tree}} = \sin(-\gamma), \quad (80)$$

which is keeping just the first term in Eq. (79), and tree level means arising from the renormalized Higgs potential, such that $\sin(-\gamma)$ is a renormalized quantity. The other terms in Eq. (79) come from bosonic and fermionic loops, hence we define the radiative shift due to loops

$$\Delta_{\text{loop}} \equiv \kappa_Z - \sin(-\gamma) = \Delta_{\text{loop}}^{\text{bosonic}} + \Delta_{\text{loop}}^{\rho_{tt}}, \quad (81)$$

where κ_Z is the renormalized scaling factor of Eq. (78), and one can identify the bosonic vs ρ_{tt} -induced top loop terms in Eq. (79). That Δ_{loop} contains both extra scalar boson loop and ρ_{tt} -induced top loop contributions is a general result, not just in the decoupling limit of Eq. (79).

Let us comment briefly on extra scalar boson loop contributions to Δ_{loop} . As we can see from Eq. (79), the magnitude of the extra scalar loop correction strongly depends on the ratio of μ_{22} and v . If $|\mu_{22}|$ is comparable to v , the loop effect provides a quadratic power-like effect as m_φ^2 . On the other hand, for $|\mu_{22}|^2 \gg v^2$, the loop effect reduces as $1/m_\varphi^2$ according to the decoupling theorem. Details of the non-decoupling effect of extra scalar loop corrections are explained in Ref. [15].

Finally, it is useful to discuss the sign for each contribution. The tree level and extra Higgs boson loop contributions decrease the hZZ coupling from the SM prediction. However, for the top quark loop effect induced by ρ_{tt} , whether the contribution attenuates or amplifies the value of the hZZ coupling depends on the sign of $\rho_{tt} \cos\gamma$. If $\rho_{tt} \cos\gamma$ is negative, the top quark loop contribution becomes the only one that increases the hZZ coupling as a main correction. But if it is positive, it would further decrease the hZZ coupling.

V. NUMERICAL CALCULATION

In our numerical calculation, we take the following parameter values as input [37]:

$$\begin{aligned}
m_Z &= 91.1876 \text{ GeV}, \quad G_F = 1.16638 \times 10^{-5} \text{ GeV}^{-2}, \\
\alpha_{\text{EM}}^{-1} &= 137.035999, \quad \Delta\alpha_{\text{EM}} = 0.06635, \\
m_t &= 173.34 \text{ GeV}, \quad m_b = 4.66 \text{ GeV}, \quad m_c = 1.27 \text{ GeV}, \\
m_\tau &= 1.77686 \text{ GeV}, \quad m_h = 125 \text{ GeV}.
\end{aligned} \quad (82)$$

Although we should investigate effects from all kinds of $\rho_{f_i f_j}$, in this paper we concentrate on investigating contributions from ρ_{tt} to the hZZ vertex for simplicity. Namely, we set $\rho_{ff} = 0$ for $f = u, c, d, s, b, e, \mu, \tau$, and $\rho_{f_i f_j} = 0$ for $i \neq j$. Contributions from the matrix components $\rho_{f_i f_j}$ ($i \neq j$) and ρ_{ff} are subdominant, as mentioned at the end of Sec. IV D. In the following numerical calculation, we set ρ_{tt} to be real for simplification of numerical calculation. We should also take into account the constraint from electroweak parameters "S, T, U" [21]. It is known that when mass differences of both extra neutral scalar bosons (H, A) and the charged scalar boson H^\pm are too large, it conflicts with the data on T parameter [22]. Therefore, we hold $m_A = m_H = m_{H^\pm}$ in the following numerical calculation. In addition, too large a deviation from 1 of $\sin(-\gamma)$ conflicts with constraint from the electroweak parameters. However, since we consider only the case of $\sin(-\gamma) > 0.98$, parameter regions considered in this paper never conflicts with the constraints of the S, T, U parameter.

We illustrate in Fig. 2 the range of variation for Δ_{loop} by scanning m_H and μ_{22} within the constraints of perturbativity and vacuum stability. We also scan $\sin(-\gamma)$, but limit the range to $0.99 \leq \sin(-\gamma) \leq 1$, as we are interested in the ρ_{tt} effect in the alignment limit. In the left (right) panel, the red, green and blue regions indicate

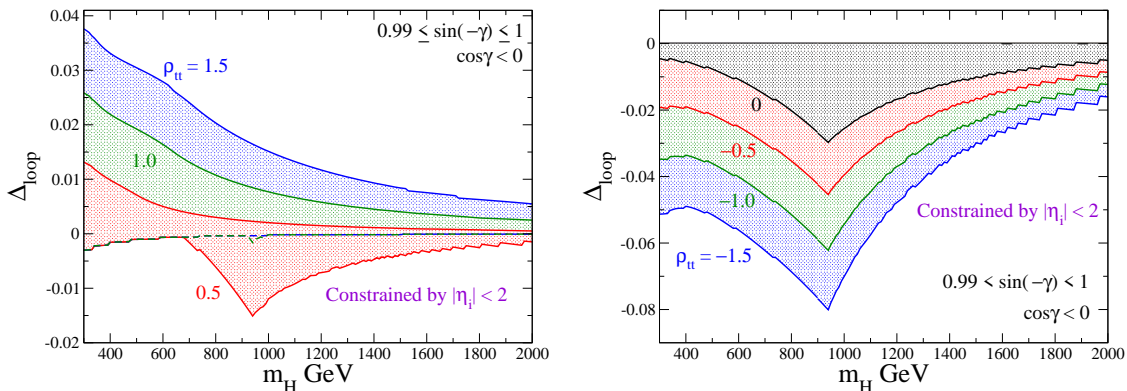


FIG. 2. Δ_{loop} vs m_H in the alignment limit, $0.99 \leq \sin(-\gamma) \leq 1$, and under perturbativity and vacuum stability constraints. The red, green and blue regions in the left (right) panel correspond to $\rho_{tt} = 0.5, 1.0, 1.5$ ($-0.5, -1.0, -1.5$), respectively.

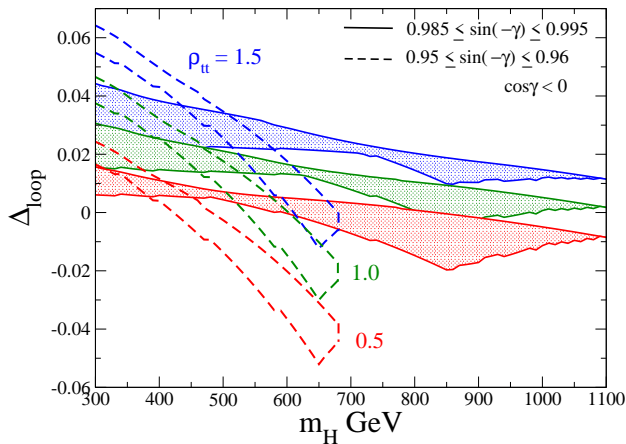


FIG. 3. Δ_{loop} vs m_H near alignment $0.985 \leq \sin(-\gamma) \leq 0.995$ (solid band) and $0.95 \leq \sin(-\gamma) \leq 0.96$ (dashed band), with settings the same as in Fig. 2.

the results for $\rho_{tt} = 0.5, 1.0, 1.5$ ($-0.5, -1.0, -1.5$), respectively. Let us try to understand the features.

The peaking of $|\Delta_{\text{loop}}|$ at $m_H \sim 950$ GeV in the right panel of Fig. 2 can be understood through the approximate formula, Eq. (79). By the non-decoupling effect of the extra scalar bosons within the perturbative bound, the strength of $|\Delta_{\text{loop}}^{\text{bosonic}}|$ ($\rho_{tt} = 0$ case) can increase as m_H^2 for moderate m_H values. But when m_H reaches 950 GeV and beyond, the perturbativity constraint ($\eta_i < 2$) cuts in, and large m_H becomes dominated by large $|\mu_{22}|$, hence Δ_{loop} shrinks toward 0 in the decoupling limit of $m_H^2 \gg v^2$. Thus, the value of 950 GeV reflects our somewhat arbitrary choice of perturbative bound, $|\eta_i| < 2$, for Higgs self-couplings. As for the effect of ρ_{tt} , since $\rho_{tt} \cos \gamma > 0$, a stronger ρ_{tt} simply allows the negative $\Delta_{\text{loop}}^{\text{bosonic}}$ effect to become even more negative.

More interesting is Fig. 2(left), where $\rho_{tt} \cos \gamma < 0$. For this case, the ρ_{tt} effect is opposite in sign to the bosonic loop contribution, and moves Δ_{loop} more positive. For

weak $\rho_{tt} = 0.5$, one sees similar peaking in negative values for Δ_{loop} as in Fig. 2(right), but for $m_H \lesssim 700$ GeV, one has $\Delta_{\text{loop}} \gtrsim 0$ as ρ_{tt} effect takes over. For larger ρ_{tt} values such as 1 or higher, Δ_{loop} is almost bound to be positive for the full m_H range, and can reach a few percent for low m_H values. For large m_H , decoupling again sets in, but more swiftly than in Fig. 2(right). All these features reflect the fact that, for $\rho_{tt} \cos \gamma < 0$, the ρ_{tt} effect competes and cancels against the bosonic loop effect, and $\Delta_{\text{loop}} \sim 0$ is allowed, which means κ_Z could still have value $\kappa_Z^{\text{tree}} = \sin(-\gamma)$.

The last statement brings about an interesting point, which we elucidate further. The properties of the 125 GeV boson h is in remarkable agreement with the SM Higgs boson, and in the 2HDM context this means we are close to alignment, i.e. $\cos \gamma \simeq 0$. The alignment limit is usually understood in terms of the decoupling limit of $m_H^2 \gg v^2$, which makes extra Higgs boson search more difficult. But could we have “alignment without decoupling” [23–25], such that the exotic Higgs bosons

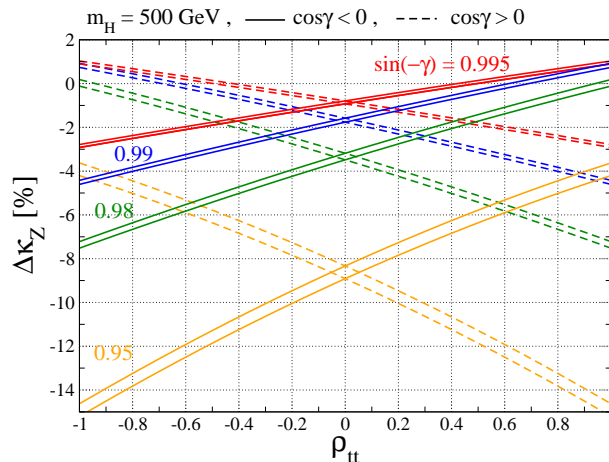


FIG. 4. $\Delta\kappa_Z$ vs ρ_{tt} for $m_H = 500$ GeV under perturbativity and vacuum stability constraints. For $\cos\gamma < 0$ ($\cos\gamma > 0$), solid (dashed) red, blue, green and orange bands are for $\sin(-\gamma) = 0.995$, 0.99, 0.98 and 0.95, respectively.

are not so heavy, making them more amenable to search? We find from our current study with potentially large ρ_{tt} and sizable exotic Higgs couplings, their effects could mutually cancel for $\rho_{tt} \cos\gamma < 0$, such that alignment is indeed “accidental”, or Nature’s design to keep the exotic Higgs doublet well hidden.

We plot Δ_{loop} vs m_H in Fig. 3 for $0.985 \leq \sin(-\gamma) \leq 0.995$ (solid band) and $0.95 \leq \sin(-\gamma) \leq 0.96$ (dashed band), where even $\sin(-\gamma) \simeq 0.955$ is still close to alignment, with $|\cos\gamma| \simeq 0.3$. The difference from Fig. 2 is that $\sin(-\gamma) = 1$ is excluded, so $\cos\gamma$ cannot vanish. One now sees the trend that, as m_H increases, Δ_{loop} extends to more negative values, until the bands are cut off by the perturbativity constraint. For the less aligned case of $\sin(-\gamma) \sim 0.955$, the drop can be as much as -0.07 , while for the closer to aligned case of $\sin(-\gamma) \sim 0.98$, the drop is milder and can be of order -0.04 . The point is that we could have $\Delta_{\text{loop}} \simeq 0$ and $\sin(-\gamma) \simeq 1$, but for moderate m_H values — alignment without decoupling. We note that, with $\sin(-\gamma)$ determined by the renormalized Higgs potential, with parameters largely not measured yet, we are far from knowing its true value, except that alignment seems to hold to good extent.

With Δ_{loop} better understood, we turn to study numerically

$$\Delta\kappa_Z \equiv \kappa_Z - 1 = [\sin(-\gamma) - 1] + \Delta_{\text{loop}}, \quad (83)$$

the deviation of the κ_Z observable of Eq. (78) from 1. First we reiterate that, e.g. for $\rho_{tt} = 1$ and for the case of $0.985 \leq \sin(-\gamma) \leq 0.995$ in Fig. 3, one has $|\Delta\kappa_Z| \lesssim 0.01$, which is rather close to alignment limit, but the full range of m_H up to TeV is allowed. We illustrate in Fig. 4 the ρ_{tt} dependence of $\Delta\kappa_Z$ for $m_H = 500$ GeV, and for $\sin(-\gamma) = 0.995, 0.99, 0.98$ and 0.95 , taking into account constraints from perturbativity and vacuum stability on Higgs sector parameters. For $\rho_{tt} = 0$, the hZZ coupling is affected by the tree level mixing effect $\sin(-\gamma) - 1$, and bosonic loop contributions $\Delta_{\text{loop}} = \Delta_{\text{loop}}^{\text{bosonic}}$. As dis-

cussed at the end of Sec. IV D, these contributions reduce the value of the hZZ coupling from SM [15]. For $\cos\gamma < 0$, the top loop contributions with negative ρ_{tt} reduce further the value of the hZZ coupling. However, if ρ_{tt} is positive, the top loop effects increase the value of the hZZ coupling, i.e. it works against the bosonic contributions. The value of $\Delta\kappa_Z$ for $\sin(-\gamma) = 0.995, 0.99$ and 0.98 turns positive at $\rho_{tt} \sim 0.5, 0.7$ and 1 , respectively, for $\cos\gamma < 0$. For $\cos\gamma > 0$, the inclination of $\Delta\kappa_Z$ is opposite to the $\cos\gamma < 0$ case.

If the hZZ coupling can be determined by experiment with some precision, we can obtain the value of ρ_{tt} for a given $\sin(-\gamma)$ value. The combined LHC Run 1 data [2] gives the 1σ range of $-6\% \leq \Delta\kappa_Z \leq 13\%$ for the hZZ coupling, which is not yet discriminating enough to obtain information on the value of ρ_{tt} , although it does disfavor $\sin(-\gamma) \lesssim 0.95$ for $\rho_{tt} \cos\gamma > 0$, i.e. an expression for alignment. With full HL-LHC data, and at future colliders such as the the ILC and the Compact Linear Collider (CLIC) [38], κ_Z is expected to be measured with higher accuracy as follows,

$$\sigma(\kappa_Z) \simeq 2\% \quad \text{HL-LHC [11]}, \quad (84)$$

$$\sigma(\kappa_Z) \simeq 0.5\% \quad \text{ILC500 [11]}, \quad (85)$$

$$\sigma(\kappa_Z) \simeq 0.8\% \quad \text{CLIC350 [39]}. \quad (86)$$

Here ILC500 means the combination of $\sqrt{s} = 250$ GeV run with L (integrated luminosity) = 250 fb^{-1} and $\sqrt{s} = 500$ GeV with $L = 500 \text{ fb}^{-1}$, while CLIC350 is the staged CLIC [38] with $\sqrt{s} = 350$ (and 380) GeV and $L = 500 \text{ fb}^{-1}$. With such precision obtainable in the future, one could extract information on ρ_{tt} within uncertainties. For example, for $m_H = 500$ GeV, if $\Delta\kappa_Z$ is measured at the central value of -5% at the HL-LHC (ILC500), $|\rho_{tt}| \simeq -0.74 \pm 0.87$ (± 0.29) and $+0.42 \pm 1.16$ (± 0.30) are implied for $\sin(-\gamma) = 0.95$ and 0.98 , respectively, where errors reflect both measurement and theoretical uncertainties. Therefore, indirect detection by hZZ coupling measurements can probe $|\rho_{tt}|$ for given value of $\sin(-\gamma)$,

while B physics experiments can place only an upper bound. We have also made clear the usefulness of an ILC, even if the energy is below H production threshold.

It is difficult to compare the constraint from indirect search with that from the direct search for H studied in Ref. [35], i.e. heavy scalar search through $gg \rightarrow H/A \rightarrow t\bar{t}$ process at HL-LHC, because the latter study corresponds to $\sin(-\gamma) = 1$ in a 2HDM. Let us compare the alignment limit (such as $\sin(-\gamma) = 0.995$) with the result of Ref. [35]. Suppose the measured central value is $\Delta\kappa_Z = 0$ at ILC500. In that case, as can be read from Fig. 4, the 2σ constraint from ILC is $-0.1 < \rho_{tt} < 1$ for $\cos\gamma < 0$ ($-1 < \rho_{tt} < 0.1$ for $\cos\gamma < 0$). The hZZ coupling precision measurement would complement direct search bound at the LHC, which gives $\rho_{tt} < 0.5$ [35], as it is hampered by complications from interference with $t\bar{t}$ background. Our comparison, however, is based on rough estimates, and we expect much progress by the time these measurements are made.

For a final perspective, we display in Fig. 5 the range of $\Delta\kappa_Z$ for a given value of ρ_{tt} , for $m_H = 500$ GeV (blue shaded) and 1000 GeV (red shaded) and close to alignment, $0.98 \leq \sin(-\gamma) \leq 1$. We take into account perturbativity and vacuum stability bounds. For $m_H = 500$ (1000) GeV, regions outside the dot-dashed (dotted) vertical lines are excluded by B_s mixing data. The dependence of $\Delta\kappa_Z$ on ρ_{tt} and $\sin(-\gamma)$ are as shown in Fig. 4. Thus, as $\Delta\kappa_Z$ for a given value of ρ_{tt} becomes more negative, $\sin(-\gamma)$ deviates more from 1 (see Eq. (83)).

We see from Fig. 5(left) that, for $\sin(-\gamma) > 0.98$, the most negative value for $\Delta\kappa_Z$ is about -7.5% for $m_H = 500$ GeV and $|\rho_{tt}| = 1$, with similar number for $m_H = 1000$ GeV and $|\rho_{tt}| = 1.5$. Such reduction of hZZ coupling can be uncovered by the HL-LHC (Eq. (84)), and would be quite interesting. However, from Fig. 4 we see that, if $\sin(-\gamma)$ is smaller in value than 0.98, such negative values for $\Delta\kappa_Z$ can be realized by non-decoupled bosonic loop effects for $\rho_{tt} = 0$. Without a clear handle on $\sin(-\gamma)$ (except that it is close to alignment), which depends on many parameters, one cannot really determine ρ_{tt} . Further measurements involving the exotic Higgs sector may help. The other direction, i.e. for $\Delta\kappa_Z > 0$, the situation is somewhat different.

We have commented that ρ_{tt} -induced top loop effects would cancel against bosonic loop effects for $\rho_{tt} \cos\gamma < 0$, which could give rise to alignment without decoupling, hence is of special interest. In order to discuss the region where $\Delta\kappa_Z \gtrsim 0$, as the possible range is narrower, we give a zoomed-in view in Fig. 5(right). Whether $m_H = 500$ GeV or 1000 GeV, in part because of the B_s mixing constraint, the hZZ coupling can at most be $\sim 1\%$ larger than the SM prediction, which HL-LHC does not have the resolution to resolve (although it can confirm a rather SM-like coupling, further supporting alignment).

The hZZ coupling, however, cannot be enhanced above SM without the ρ_{tt} effect of top loop diagrams. Therefore, if such deviation is measured in future precision measurements such as at the ILC500, it can probe

the ρ_{tt} coupling in the general 2HDM. For example, suppose $\Delta\kappa_Z$ is measured with central value $+1.5\%$ at the ILC500 or CLIC350. We mark this as a purple horizontal solid line in Fig. 5(right), with dashed and dot-dashed horizontal lines indicating 2σ error bars at the ILC500 and CLIC350 (Eqs. (85) and (86)), respectively. In this case, $|\rho_{tt}| \lesssim 0.65$ (0.9) is excluded by 2σ for $m_H = 500$ (1000) GeV by the ILC500, pointing towards an extra ρ_{tt} Yukawa interaction. Of course, if the central value falls at 1.0, then more data would be needed. We remark that the comparison of CLIC350 with ILC500 is also an issue of optimizing collision energy and run time. If an evident deviation in the hZZ coupling is not measured by the future precise measurement, we are hopeful for exploration for ρ_{tt} by additional Higgs bosons searches using the signal $gg \rightarrow H/A \rightarrow t\bar{t}$ at the HL-LHC experiment [35].

VI. CONCLUSION

We have calculated the renormalized hZZ coupling at the one-loop level by the on-shell and minimal subtraction scheme in the general 2HDM without Z_2 symmetry. We numerically evaluated the one-loop corrected scaling factor of the hZZ coupling, in order to investigate the ability of indirect detection of extra Yukawa interactions with future Higgs boson coupling measurements. In this paper, we focused on the top quark loop contributions and heavy scalar boson loop contributions for simplicity.

By deriving an approximate formula for the renormalized scaling factor κ_Z of the hZZ coupling, we make explicit that the value of κ_Z is determined by ρ_{tt} , the mass of extra scalar bosons m_φ , $\sin(-\gamma)$ and the sign of $\cos\gamma$. Since κ_Z would be $\sin(-\gamma)$ if one considers only the renormalized Higgs potential, we evaluate how much $\kappa_Z - \sin(-\gamma)$ is shifted by radiative corrections in the alignment limit of $\sin(-\gamma) \simeq 1$. We scan m_H and μ_{22} keeping the assumption $m_H = m_A = m_{H^\pm}$ under the constraints of perturbativity and vacuum stability for some representative ranges for $\sin(-\gamma)$. We find that the bosonic one-loop corrections always shift $\kappa_Z - \sin(-\gamma)$ in the negative direction, while the top loop correction induced by ρ_{tt} depends on the sign of $\rho_{tt} \cos\gamma$. For $\rho_{tt} \cos\gamma > 0$, the ρ_{tt} effect also shifts $\kappa_Z - \sin(-\gamma)$ in the negative direction, but for $\rho_{tt} \cos\gamma < 0$, the top loop effect shifts $\kappa_Z - \sin(-\gamma)$ in the *positive* direction, and can cancel against the bosonic effect. We have checked numerically that the magnitude of radiative shift tends to vanish in the decoupling limit of $m_\varphi \rightarrow \infty$.

The cancellation effect mentioned above illustrates alignment without decoupling. With $\kappa_Z - \sin(-\gamma)$ kept small by this cancellation, even when both $|\rho_{tt}|$ and extra Higgs self-couplings are $O(1)$ or larger, the observed ‘‘alignment’’ may be accidental, and that exotic Higgs bosons could be around several hundred GeV in mass, rather than the usual perception that alignment is realized by the decoupling limit of very heavy exotic Higgs. This makes the general 2HDM rather interesting.

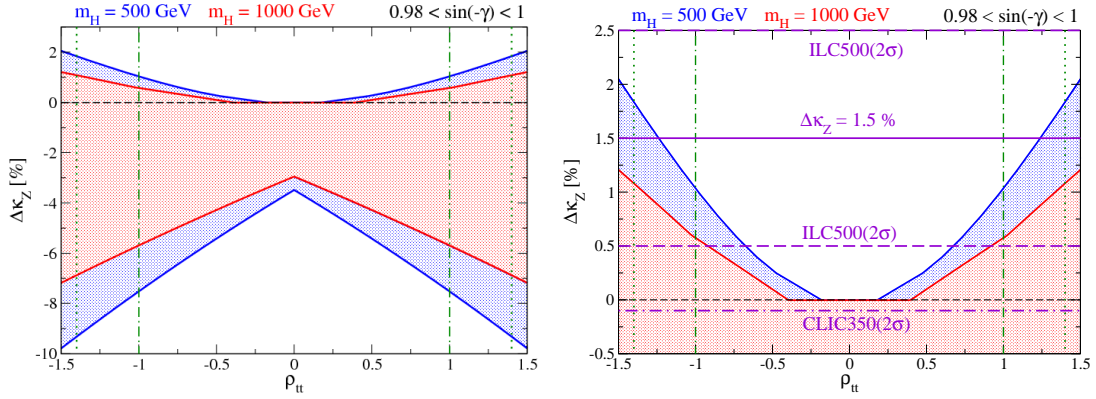


FIG. 5. Range of $\Delta\kappa_Z$ for a given ρ_{tt} value in the alignment limit, $0.98 \leq \sin(-\gamma) \leq 1$, and under perturbativity and vacuum stability constraints. Blue (red) region is for $m_H = 500$ (1000) GeV, with ρ_{tt} outside of dot-dashed (dotted) vertical lines excluded by B_s mixing. In the right panel, which is a zoomed-in view for $\Delta\kappa_Z \gtrsim 0$, a horizontal solid line shows a favorable central value of $\Delta\kappa_Z$, with horizontal dashed (dot-dashed) lines indicating 2σ error bars at the ILC500 (CLIC350).

Future precision measurements such as at the ILC (and even the HL-LHC) can survey $|\rho_{tt}|$ when hZZ coupling is significantly lower than one, for each value of $\sin\gamma$ and m_ϕ , while B physics experiments and direct search of heavy scalar bosons at LHC can place only upper bounds on $|\rho_{tt}|$. However, given that bosonic corrections reduce the hZZ coupling also, if $\sin(-\gamma)$ is less than, say 0.98, one may not be able to tell apart a purely bosonic effect, or that from ρ_{tt} . But we have numerically showed that the hZZ coupling cannot be larger than the SM predicted value without the ρ_{tt} -induced top quark loop effect, although the effect is at the percent level. If the hZZ coupling turns out to be 1% or more larger than the SM value, the deviation can be sensed by the precision measurement at the ILC, and would be definite evidence of the extra Yukawa interaction. But the run time needed may exceed the definition of ILC500. Of course, a higher energy ILC (or CLIC) could possibly discover the exotic heavy Higgs bosons directly, in this interesting case of alignment without decoupling.

Although we took into account the effect of extra Yukawa interaction for only the top quark, other fermion loop effects arising from extra Yukawa interactions should also be evaluated. For example, the effect of ρ_{cc} has not been explored much by B physics and LHC experiments. Furthermore, we should investigate not only the effects of the real part of ρ_{ij} , which is what is studied in this paper for simplicity, but we should also explore the impact of the imaginary part. The imaginary parts, or CP phases of ρ_{ij} could be of essential importance for the generation of matter-antimatter asymmetry of the Universe.

ACKNOWLEDGMENT

We thank M. Kohda for discussions. WSH is supported by grants MOST 104-2112-M-002-017-MY2, MOST 105-2112-M-002-018 and NTU 105R8965, and MK is supported by MOST 106-2811-M-002-010.

Appendix A: 1PI diagram contributions

We give fermion loop contributions to the tadpoles, the two-point functions and the three point functions at the one-loop level by using Passarino-Veltman functions [36] whose notation is same as those in Ref. [40]. Explicit forms of 1PI bosonic loop contributions necessary for the renormalized hZZ coupling are given in Ref. [15].

The 1PI tadpole diagrams for h , H are calculated by

$$T_{h,F}^{1PI} = \sum_f \frac{4N_f^C}{16\pi^2} \lambda_{hff} m_f A[m_f], \quad (\text{A1})$$

$$T_{H,F}^{1PI} = \sum_f \frac{4N_f^C}{16\pi^2} \lambda_{Hff} m_f A[m_f], \quad (\text{A2})$$

where N_f^C indicates the color factor of f , and explicit formulae of $\lambda_{\phi ff}$ are given in Eqs. (22) and (23).

The two-point function of h and h - H mixing are cor-

rected by the following 1PI diagrams,

$$\begin{aligned} \Pi_{hh,F}^{1\text{PI}}[p^2] = & -\frac{4N_f^C}{16\pi^2} \left\{ (\lambda_{hff})^2 A[m_f] \right. \\ & + \frac{1}{2} (\lambda_{hff})^2 [4m_f^2 - p^2] B_0[p^2; m_f, m_f] \\ & - \frac{1}{2} (\delta_f^h)^2 [2A[m_f] - p^2 B_0[p^2; m_f, m_f]] \left. \right\} \\ & - \frac{N_i^C \cos^2 \gamma}{32\pi^2} \left\{ 2\rho_{ij}^A m_i m_j B_0[p^2; m_i, m_j] \right. \\ & + \rho_{ij}^B [A[m_i] + A[m_j] \\ & \left. + (m_i^2 + m_j^2 - p^2) B_0[p^2; m_i, m_j]] \right\}, \quad (\text{A3}) \end{aligned}$$

$$\begin{aligned} \Pi_{hH,F}^{1\text{PI}}[p^2] = & -\frac{4N_f^C}{16\pi^2} \left\{ \lambda_{hff} \lambda_{Hff} A[m_f] \right. \\ & + \frac{1}{2} \lambda_{hff} \lambda_{Hff} [2m_f^2 - p^2] B_0[p^2; m_f, m_f] \\ & - \frac{1}{2} \delta_f^h \delta_f^H [2A[m_f] - p^2 B_0[p^2; m_f, m_f]] \left. \right\} \\ & - \frac{N_i^C}{32\pi^2} \sin \gamma \cos \gamma \left\{ 2\rho_{ij}^A m_i m_j B_0[p^2; m_i, m_j] \right. \\ & + \rho_{ij}^B [A[m_i] + A[m_j] \\ & \left. + (m_i^2 + m_j^2 - p^2) B_0[p^2; m_i, m_j]] \right\}, \quad (\text{A4}) \end{aligned}$$

where ($i \neq j$)

$$\delta_f^h = -\frac{\cos \gamma}{2\sqrt{2}} (\rho_{ff} - \rho_{ff}^*), \quad (f = t, b, c, s, u, d) \quad (\text{A5})$$

$$\delta_f^H = -\frac{\sin \gamma}{2\sqrt{2}} (\rho_{ff} - \rho_{ff}^*), \quad (f = t, b, c, s, u, d) \quad (\text{A6})$$

$$\rho_{ij}^A = \rho_{ij} \rho_{ji} + \rho_{ij}^* \rho_{ji}^*, \quad (\text{A7})$$

$$\rho_{ij}^B = \rho_{ij} \rho_{ij}^* + \rho_{ji} \rho_{ji}^*. \quad (\text{A8})$$

The 1PI diagram contributions to the hZZ and HZZ vertex form factors defined in Eq. (71) are given by

$$\begin{aligned} \Gamma_{\phi ZZ}^{1,1\text{PI}}(p_1^2, p_2^2, q^2) = & -\sum_F \frac{8N_f^C m_f m_Z^2}{16\pi^2 v^2} \lambda_{\phi ff} \times \\ & \left\{ (v_f^2 + a_f^2) \left[(3p_1^2 + p_1 \cdot p_2) C_{11} + (3p_1 \cdot p_2 + p_2^2) C_{12} \right. \right. \\ & + 2p_1^2 C_{21} + 2p_2^2 C_{22} + 4p_1 \cdot p_2 C_{23} + 2(D-2) C_{24} \left. \right] \\ & - (v_f^2 + a_f^2) \left[(p_1^2 + p_1 \cdot p_2) C_{11} + (p_1 \cdot p_2 + p_2^2) C_{12} \right. \\ & \left. \left. + p_1^2 C_{21} + p_2^2 C_{22} + 2p_1 \cdot p_2 C_{23} + (D-2) C_{24} \right] \right\}, \quad (\text{A9}) \end{aligned}$$

where $D = 4 - \epsilon/2$, $C_{ij} \equiv C_{ij}[p_1^2, p_2^2, q^2; m_t]$, and $v_f = I_f - \sin^2 \theta_W Q_f$ and $a_f = I_f$ are the vector and axial vector coupling coefficients of the Zff vertex.

-
- [1] G. Aad *et al.* [ATLAS and CMS Collaborations], Phys. Rev. Lett. **114**, 191803 (2015).
[2] G. Aad *et al.* [ATLAS and CMS Collaborations], JHEP **1608**, 045 (2016).
[3] S.L. Glashow and S. Weinberg, Phys. Rev. D **15**, 1958 (1977).
[4] See, e.g. G.C. Branco, H.R.C. Ferreira, A.G. Hessler and J.I. Silva-Marcos, JHEP **1205**, 001 (2012), and references therein.
[5] H. Fritzsch, Phys. Lett. **73B**, 317 (1978).
[6] T.-P. Cheng and M. Sher, Phys. Rev. D **35**, 3484 (1987).
[7] W.-S. Hou, Phys. Lett. B **296**, 179 (1992).
[8] K.-F. Chen, W.-S. Hou, C. Kao and M. Kohda, Phys. Lett. B **725**, 378 (2013).
[9] R. Harnik, J. Kopp and J. Zupan, JHEP **1303**, 026 (2013).
[10] B. Altunkaynak, W.-S. Hou, C. Kao, M. Kohda and B. McCoy, Phys. Lett. B **751**, 135 (2015).
[11] S. Dawson *et al.*, arXiv:1310.8361 [hep-ex].
[12] ATLAS Collaboration, ATL-PHYS-PUB-2014-016.
[13] S. Kanemura, Y. Okada, E. Senaha and C.-P. Yuan, Phys. Rev. D **70**, 115002 (2004).
[14] S. Kanemura, M. Kikuchi and K. Yagyu, Phys. Lett. B **731**, 27 (2014).
[15] S. Kanemura, M. Kikuchi and K. Yagyu, Nucl. Phys. B **896**, 80 (2015).
[16] A. Arhrib, R. Benbrik, J. El Falaki and A. Jueid, JHEP **1512**, 007 (2015).
[17] M. Krause, R. Lorenz, M. Muhlleitner, R. Santos and H. Ziesche, JHEP **1609**, 143 (2016).
[18] M. Krause, M. Muhlleitner, R. Santos and H. Ziesche, arXiv:1609.04185 [hep-ph].
[19] A. Arhrib, R. Benbrik, J. El Falaki and W. Hollik, arXiv:1612.09329 [hep-ph].
[20] S. Kanemura, M. Kikuchi and K. Sakurai, Phys. Rev. D **94**, 115011 (2016).
[21] M. E. Peskin and T. Takeuchi, Phys. Rev. D **46**, 381 (1992).
[22] S. Kanemura, Y. Okada, H. Taniguchi and K. Tsumura, Phys. Lett. B **704**, 303 (2011) [arXiv:1108.3297 [hep-ph]].
[23] J.F. Gunion and H.E. Haber, Phys. Rev. D **67**, 075019 (2003).
[24] P. S. Bhupal Dev and A. Pilaftsis, JHEP **1412**, 024 (2014) Erratum: [JHEP **1511**, 147 (2015)] [arXiv:1408.3405 [hep-ph]].
[25] N. Craig, J. Galloway and S. Thomas, arXiv:1305.2424 [hep-ph].
[26] S. Davidson and H.E. Haber, Phys. Rev. D **72**, 035004 (2005).

- [27] H.E. Haber and D. O'Neil, Phys. Rev. D **74**, 015018 (2006).
- [28] I.P. Ivanov, Phys. Rev. D **75**, 035001 (2007).
- [29] A. Crivellin, A. Kokulu and C. Greub, Phys. Rev. D **87**, 094031 (2013).
- [30] V. Khachatryan *et al.* [CMS Collaboration], Phys. Lett. B **749**, 337 (2015).
- [31] G. Aad *et al.* [ATLAS Collaboration], JHEP **1512**, 061 (2015).
- [32] V. Khachatryan *et al.* [CMS Collaboration], JHEP **1702**, 079 (2017).
- [33] S. Chatrchyan *et al.* [CMS Collaboration], Phys. Rev. Lett. **111**, 211804 (2013) Erratum: [Phys. Rev. Lett. **112**, 119903 (2014)].
- [34] G. Aad *et al.* [ATLAS Collaboration], JHEP **1508**, 148 (2015).
- [35] M. Carena and Z. Liu, JHEP **1611**, 159 (2016).
- [36] G. Passarino and M.J.G. Veltman, Nucl. Phys. B **160**, 151 (1979).
- [37] C. Patrignani *et al.* [Particle Data Group Collaboration], Chin. Phys. C **40**, 100001 (2016).
- [38] M.J. Boland *et al.* [CLIC and CLICdp Collaborations], arXiv:1608.07537 [physics.acc-ph].
- [39] H. Abramowicz *et al.*, arXiv:1608.07538 [hep-ex].
- [40] K. Hagiwara, S. Matsumoto, D. Haidt and C.S. Kim, Z. Phys. C **64**, 559 (1994) Erratum: [Z. Phys. C **68**, 352 (1995)].